Topics in Catalysis
https://doi.org/10.1007/s11244-019-01172-3

ORIGINAL PAPER

Oleic Acid Esterification Catalyzed by Zeolite Y-Model of the Biomass Conversion

Glaucio J. Gomes[1,3] · Daniel M. Dal Pozzo[4] · María Fernanda Zalazar[1,2] · Michelle Budke Costa[4] · Pedro Augusto Arroyo[3] · Paulo R. S. Bittencourt[4]

Abstract
Residual oils and fats are promising renewable sources for the production of liquid fuels and the synthesis of various chemicals with significant life cycle and large-scale economic advantages over other biomass sources. Thus, oleic acid esterification was investigated on zeolites type FAU and sulfuric acid by kinetic, spectroscopic assessments and theoretical calculations using a hybrid ONIOM scheme. In the catalytic tests, the solid catalyst with the highest Si/Al (H-Y-80) ratio showed the highest catalytic activity for esterification (92% conversion) as compared to H-Y-5.2 (66% conversion), Na-Y (15% conversion) and homogeneous acid catalysis (89% conversion). The catalytic activity between different acid catalysts is discussed. It was observed that the acidity of the active sites and the hydrophobicity resulting from the Si/Al molar ratio influence the esterification conversion. Theoretical calcultations predicts that the voluminous confined space of the FAU zeolite perfectly accommodates the oleic acid molecule in the adsorption step ($E_{ads} = -25.5$ kJ mol^{-1}) and the van der Waals interactions of the zeolite walls with the aliphatic chain help to accommodate the bulky molecule between the supercages. Experimental and theoretical results confirm that H-Y-80 zeolite applied in the esterification reaction can be an efficient catalyst in processes involving conversion of unsaturated fatty acids.

Keywords Green chemistry · Oleic acid adsorption · Solid acid catalyst · Density functional theory · Confinement effects

1 Introduction

Lignocellulosic biomass, starches, vegetable oils and animal fats are very promising renewable sources for the production of liquid and chemical fuels with significant life cycle and advantages of economies of scale over other biomass sources, however the structural nature of these molecules determines the routes transformation needed to value and convert carbon content into products of industrial interest [1]. Changes in the global challenges of energy, carbon (raw materials) and the environment (pollution control) are demanding innovative solutions in which material science and catalytic technology will play a crucial role in addressing key issues involving green chemistry [2].

Carboxylic acids esterification is a very used reaction for the chemical industry, mainly in the biofuels production, but it is highly dependent on the use of mineral and inorganic compounds (e.g., H_2SO_4, HCl, HI and others), which require expensive and energy intensive water treatments [3, 4]. In the green chemistry scenario, the development of non-corrosive and recoverable acidic solid catalysts used in the

✉ María Fernanda Zalazar
mfzalazar@conicet.gov.ar

✉ Pedro Augusto Arroyo
arroyo@uem.deq.br

[1] Laboratorio de Estructura Molecular y Propiedades, Facultad de Ciencias Exactas, Naturales y Agrimensura, Universidad Nacional del Nordeste (UNNE), Avenida. Libertad 5460, 3400 Corrientes, Argentina

[2] Instituto de Química Básica y Aplicada del Nordeste Argentino, IQUIBA-NEA, CONICET-UNNE, Avenida Libertad 5460, 3400 Corrientes, Argentina

[3] Laboratórios de Catálise Heterogênea e Biodiesel (LCHBio), Universidade Estadual de Maringá (UEM), Avenida Colombo, 5790-Jardim Universitário, Maringá, Paraná CEP: 87020-900, Brazil

[4] Laboratório de Análise Térmica e Espectroscopia de Combustíveis e Materiais, Universidade Tecnológica Federal do Paraná (UTFPR), Avenida Brasil 4232, Medianeira 85884-000, Brazil

Published online: 22 April 2019

esterification reaction efficiently is therefore highly desirable for improving the process by bypassing the generation of large amounts of typically produced wastes [5, 6].

A wide range of acid and basic heterogeneous catalysts for free fatty acids (FFA) esterification and triacylglyceride (TAG) transesterification have been recently developed and extensively reviewed by different researchers [6–10]. However zeolites stand out in catalytic processes based on their strong and tunable acidity, microporous dimension allowing control of molecular traffic and high reaction surface areas, its robustness and high thermal stability, leading to easy regeneration at high temperatures, and finally nature adjustable so that match the need for chemical transformation [11–13].

Zeolite acidity has been the subject of intense debate on the different mechanisms that guide the esterification reaction. Many studies [4, 14, 15] indicate that the reaction of esterification in acidic zeolites occurs preferentially by the Eley–Rideal mechanism favoring initially the adsorption of the acid on the surface of the catalyst, other studies suggest that the mechanism of Langmuir–Hinshelwood is preferred. Bedard et al. [16], demonstrated that between the different stages of the reaction, the presence of an intermediate formed by acetic acid and ethanol could be found in different types of zeolites. Recently, from the molecular viewpoint, it was evaluated the adsorption and coadsorption steps of acetic acid and MeOH on the H-Beta zeolite and was observed that the adsorption complex involving the sharing of the proton by both reactants in a single step is extremely strong when compared to the adsorption by a single molecule [17].

Various studies involving protonated zeolites show that besides the discussion about the adsorption mechanism, the structural topology of different zeolites makes it impossible to apply for the esterification of bulky reagents due to the shape-selectivity that controls the diffusion process in the micropores [18–21]. However, different research groups in order to determine the effect of different acidic zeolites on the esterification [14, 15, 22–28] using reaction temperatures in the range of 60–130 °C with low carboxylic acid:alcohol molar ratios (1:1–1:9), have shown that acid strength, channel structure and hydrophobicity can beneficially influence the formation of products. These results presented in the literature contrast with some studies that suggest that microporous materials are suitable for esterification reactions of bulky acids as in the case of oleic acid (OAc) which can be considered as a biomass conversion model, because it is present in several raw materials derived from biomass.

Among the different zeolite framework topologies, Faujasite (FAU type zeolite) has large pores diameter (0.74–0.8 nm) [29, 30] that can be used to accommodate bulky fatty acids between its large supercages. Corma et al. [31] investigated the esterification of phenols in hierarchical H-Y and observed that adjusting the Si/Al ratio, the solid acid catalyst activate the reaction very similar to H_2SO_4, similar results were presented by Kirumakki [14, 15]. However, it should be noted that esterification reactions at temperatures of 60–70 °C result in the formation of water, which alters the reaction equilibrium for less product formation, so it is necessary to carry out the esterification reaction near 150 °C, removing water from the reaction medium by evaporation [32].

Doley et al., [28, 33] obtained good conversions in the esterification of OAc on H-Y prepared from kaolin, under mild conditions. Similar results were also presented recently [27] for the esterification of palmitic acid on H-Y, suggesting that the pore size and hydrophobicity/hydrophilicity balance, rather than acid site properties are critical for efficient esterification of bulky fatty acids. However, experimental and theoretical studies involving unsaturated fatty acids and their relationship with pore and cavity sizes in the crystalline structures of zeolites are necessary in order to obtain valuable information on the role of the confinement effect and the catalytic activity in chemical reactions involving processes of conversion of biomass. Thus, in this work was reported a study on the esterification of oleic acid on different FAU-type zeolites and compare it with the homogeneous acid catalysis, theoretical calculations are used as a support to relate the size of the limiting reactant to the catalyst structure explaining the adsorption of OAc into the pores and cavities.

2 Experimental

FAU zeolites ($NH_4^+ - Y$, $Si/Al_{tot} = 80$, 780 $m^2\ g^{-1}$; $NH_4^+ - Y$, $Si/Al_{tot} = 5.2$, 660 $m^2\ g^{-1}$) were purchased from Zeolytes International. Zeolite materials were calcined at 550 °C for 3 h under N_2 flow in a multi-purpose unit, yields the H-Y-80 and H-Y-5.2 zeolites used in the reaction. The Na-Y zeolite ($Si/Al_{tot} = 2.6$, 789 $m^2\ g^{-1}$) was obtained from FCC S. A. (Fábrica Carioca de Catalisadores S. A.). It was subjected to calcination at 550 °C for 3 h. Sulfuric Acid (H_2SO_4,) was used as the homogeneous catalyst for comparison of yields with the FAU type heterogeneous catalysts.

The chemical characterization of these materials was accomplished by ATR, using a PerkinElmer Spectrum 100 Spectrometer. The spectra were acquired in the range of 4000–600 cm^{-1}, averaging 128 scans, at a resolution of 2 cm^{-1}.

Temperature-programmed desorption of ammonia (NH_3-TPD) was performed in a Quantachrome Instruments Chembet-3000. First, about 200 mg of the sample was thermally treated at 300 °C in a vacuum, using a N_2 stream, for 1 h. Next, NH_3 was adsorbed at 100 °C for 30 min using a stream mixture of 5% NH_3 in N_2. Next, an N_2 purge stream was used for 2 h, to remove all the physically adsorbed NH_3.

NH_3 was chemically desorbed by increasing the temperature at a rate of 10 °C min^{-1} from 100 to 600 °C.

TGA-DTA analysis was carried out in a PerkinElmer STA 6000 Thermo-Analyzer, 20 mg of catalyst was packed in a platinum crucible. The samples were stabilized at 100 °C by 5 min and then heated to 750 °C at a heating rate of 10 °C min^{-1}, in a flow of 20 mL min^{-1} of N_2.

Reactions were carried out in a glass stirred reactor connected to a condenser. All experiments were conducted at the same conditions of a 1:3 molar ratio of OAc to MeOH, 10 wt% catalyst, 100 °C and 800 rpm. The non-catalytic reaction was tested in the same conditions. The reaction time was 5 h, starting after the temperature reached the set point and the agitation commenced. During the reaction, samples were extracted at 0, 15, 30, 60, 90, 120, 150, 180, 240, and 300 min. Also, a non-catalytic reaction was performed to verify the contribution of non-catalytic esterification to the ethyl ester yield. Samples (50 µL) of the reaction medium were collected and diluted with 1 mL of hexane in a vial for further gas chromatograph with a flame ionization detector (GC-FID, Shimadzu GC 2010 Plus).

3 Theoretical Methods

The catalyst cluster was obtained using crystallographic information [30]. The unit cell of the cluster was extended and trimmed using the Zeobuilder software [34]. The structure of the FAU-type aluminosilicate was modeled from a cluster large enough to accommodate an OAc molecule inside the cavity and relate their topological characteristics to the size of the reagent (Fig. 1).

Hydrogen atoms were added in bonds cut to stabilize the structure and avoid dangling bonds, at a bond length of 1.47 Å along the terminal Si–O groups. The Brønsted acid site was introduced into the model by replacing a Si atom by Al in the O1H position [30]. The resulting cluster model has a total of 642 atoms with an overall composition of $AlH_{137}O_{314}Si_{190}$. The H-Y structure was optimized using the ONIOM scheme developed by Morokuma and coworkers [35, 36], at M06-2X/6-31G (d): PM6 level. This methodology was used in our previous work [37].

The model is defined as 11T/200T, being 11T (T = Si or Al atom) the high layer that represents the active site and the neighboring atoms that are relaxed during the optimization, while the remaining atoms of the 200 T model in the lower layer are fixed at their respective crystallographic positions. The optimization calculation was performed using the Gaussian 09 program package [38]. The stationary points were characterized by calculating the Hessian matrix and analyzing the normal vibrational modes.

4 Results and Discussion

4.1 Catalyst Characterization

Figure 2 shows the ATR spectroscopy analysis of zeolites H-Y-80, H-Y-5.2 and Na-Y, which are in agreement with the literature [39]. The spectrum shows six bands signal at 3413, 1637, 1186, 978, 823, 709 cm^{-1}. Vibration bands at 709, 823 and 978 cm^{-1}, corresponding to the formation structure of the catalysts. According to Salman et al., [40] systematic changes in spectra shapes are observed with increasing temperature over the bending, symmetrical and asymmetric stretching vibrations of the TO_4 units between 700–900 and 900–1200 cm^{-1}.

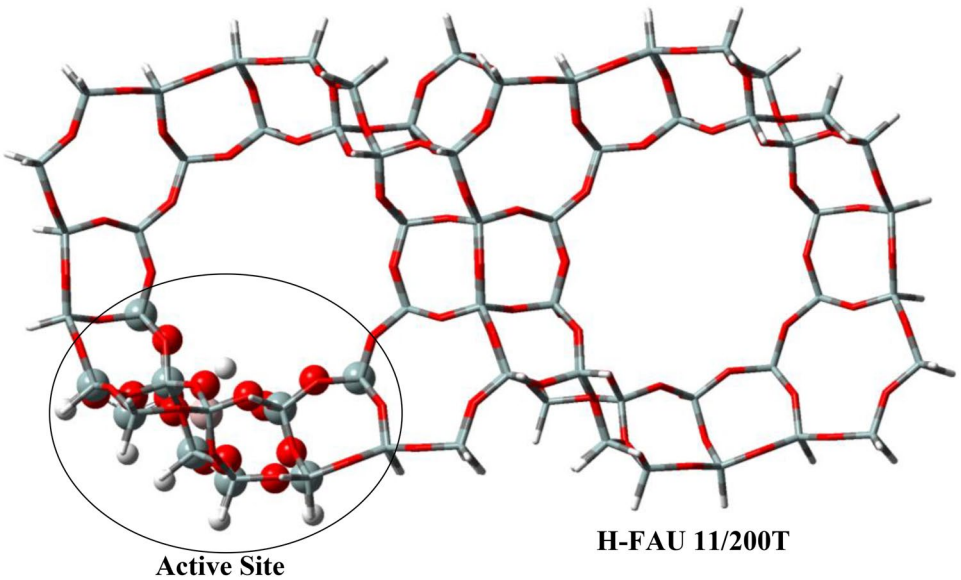

Fig. 1 Large cluster view of the H-FAU zeolite structure. The ball-and stick highlighted part refers to the 11-membered TO_4 ring including the Brønsted acidic site adopted as the model for the high-level (M06-2X) calculations for the hybrid ONIOM M06-2X/6-31G (d):PM6. Color key: H in white, Si in gray, O in red and Al in pink

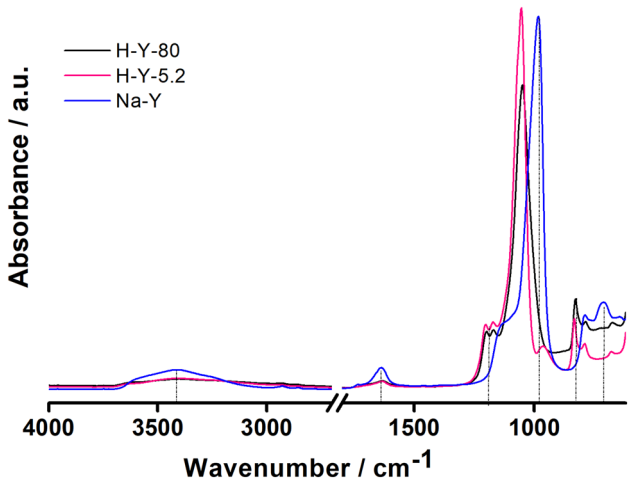

Fig. 2 IR spectra of H-Y zeolites samples after evacuation at 50 °C, in the region 4000–600 cm^{-1}

Bands at 978 and 1180 cm^{-1} are characteristic in aluminosilicates, as these bands have a correlation with asymmetric stretches O–T–O, and the vibrations found in these regions are linear with the alumina framework. Zhao et al. [41], demonstrated that the 1050 and 706 cm^{-1} bands represent the asymmetric and symmetrical stretch vibrations corresponding to the internal structure of TO_4, while the bands at 1170 and 788 cm^{-1} represent the asymmetric and symmetrical stretching vibrations corresponding to the external structure of TO_4. The difference of the intensity in the O–T–O region for H-Y-80 and H-Y-5.2 refers to the Si/Al ratio.

For all FAU aluminosilicates, the presence of adsorbed water was verified by the bands at 1637 cm^{-1} (axial deformation of δOH) and 3413 cm^{-1} (νOH stretching). However, it was observed that Na-Y zeolite had a higher intensity in these bands due to the presence of Na^+ ions in the catalyst structure. In fact, it has been shown that water adsorbs relatively strongly over the Na-Y surface [42].

Characterization of the thermal stability in the activation of H-Y-80, H-Y-5.2 and Na-Y zeolites was performed by TGA-dTG, and the thermogravimetric profile was analyzed (Fig. 3), showing that all solid catalysts have similar thermal stability over TGA curve, but with different mass losses.

Two processes of mass loss were more accurately identified by dTG: (i) the first process refers to the desorption of water molecules adsorbed on the surface of the catalytic solids between 100 and 350 °C. (ii) the second process occurs at over a wide temperature range (400–670 °C), being related to simultaneous desorption processes of NH_3, Na^+, NH_4^+ and hydroxylation, similar results for aluminosilicates are identified by other authors [17, 42].

However, H-Y-80 zeolite maintains adsorbed water at higher temperatures when compared to H-Y-5.2 and Na-Y, having higher thermal stability due to high Si/Al ratio, which results in more distant active sites distributed along the surface of the catalyst and in turn this effect contributes to stronger adsorption on the active sites. Na-Y and H-Y-5.2 zeolites are more hydrophilic materials, due to the greater presence of Al in the structure [43].

Acid properties of the H-Y-80, H-Y-5.2 and Na-Y zeolites were evaluated by NH_3-TPD, as shown in Fig. 4, since the Si/Al ratio considerably change the amount of acid sites on the catalyst [23, 29, 44]. DTG desorption peaks observed at 165–194 °C were attributed to weak acid sites or ammonia physically adsorbed on Si–OH sites (external silanol groups), while strong acid sites were identified between 302 and 327 °C.

The H-Y-80 and H-Y-5.2 zeolites presented a similar TPD profile, in which two peaks referring to the weak and strong acid sites of each material can be identified. However, H-Y-80 has stronger acid sites identified by the intensity of the band at 327 °C (strong sites) with high intensity when compared to H-Y-5.2 that has a higher intensity in the band of 194 °C (weak sites). This indicates that the acidic sites in the pore interior are in a higher amount in H-Y-80 favoring the greater catalytic activity inside the pores and cavities. In the

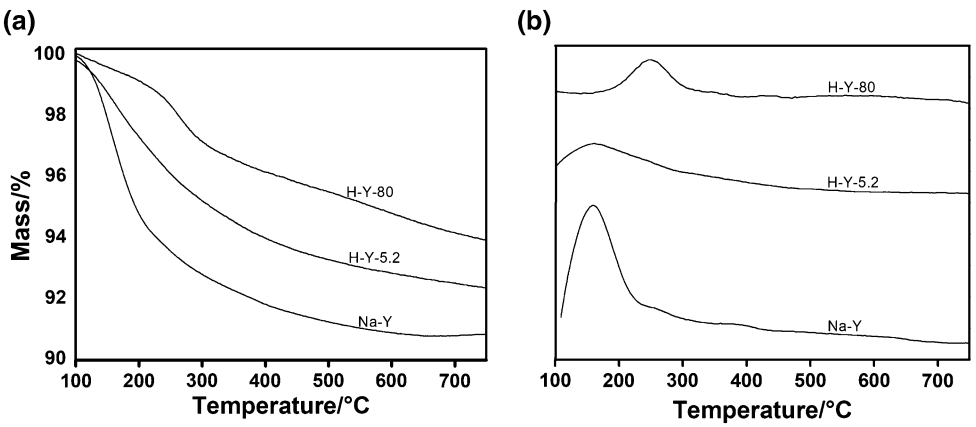

Fig. 3 TGA **a** and dTG **b** curves of H-Y zeolites. Conditions: N_2 flow of 20 mL min^{-1}; Temperature range from 100 to 750 °C with a heating rate of 10 °C min^{-1}

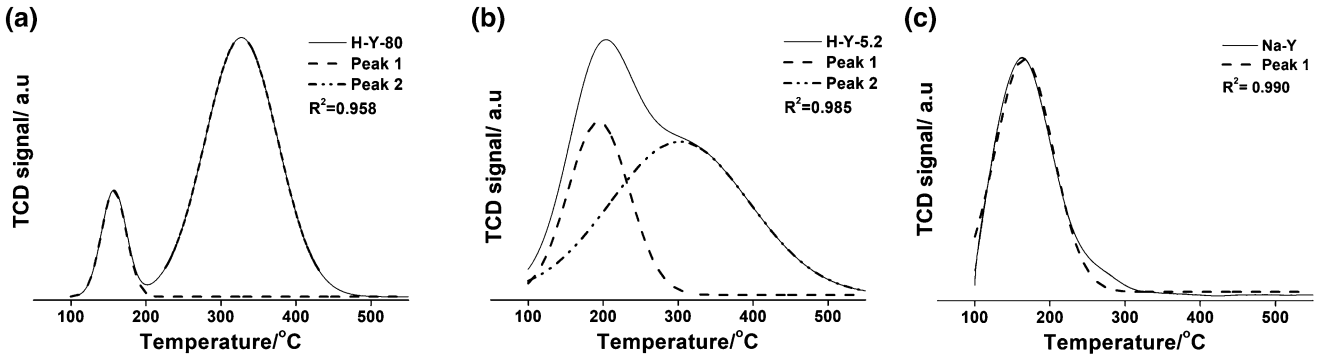

Fig. 4 Experimental and deconvolution of NH_3-TPD peaks of H-FAU zeolites. Conditions: Temperature range from 100 to 550 °C

case of the Na-Y zeolite, no strong sites were observed, however the band centered at 165 °C shows an acidity behavior similar to the first peak of zeolite H-Y-5.2, the absence of strong acidity in zeolite H-Y was demonstrated by Mistry et al. [45] in a catalyst with lower catalytic activity and higher Si/Al molar ratio.

5 Catalytic Evaluation

Figure 5 shows the conversion of OAc to methyl oleate on H-Y-80, H-Y-5.2, Na-Y and H_2SO_4, as a comparison, a non-catalyst reaction was performed to observe the self-catalytic effect of OAc and MeOH.

Among the solid catalysts (H-Y-80, H-Y-5.2 and Na-Y), the higher catalytic activity was observed by H-Y-80 zeolite with a conversion of 92% of methyl esters after 180 min of reaction. Similar results are observed by Prinsen et al. [27] in the esterification of palmitic acid (straight chain) on H-Y-60. However, the OAc used in this work is more voluminous and unsaturated which results in a larger diffusion process inside the pores. Catalytic results between the solid (H-Y-80, H-Y-5.2 and Na-Y) and homogeneous (H_2SO_4) catalysts show that the hydrophobicity effect of materials with high Si/Al ratio is interesting for the esterification process. Our results (Fig. 5) indicate that conversions above 180 min for H-Y-80 are stable, whereas the deactivation of H_2SO_4 is clearly observed over time.

For zeolite H-Y-5.2, full conversion of 66% was observed after 180 min of reaction. Comparison of the protonated zeolites (H-Y-80 and H-Y-5.2) clearly shows a significant difference after the time of 60 min, on the reaction rate of both catalysts. It was observed that H-Y-5.2 had a higher amount of weak acid sites (Si–OH) when compared to H-Y-80 and that the Brønsted acid sites were in a lower amount (Fig. 4). This result indicates that the reaction on H-Y-5.2 is affected by the high density of acid sites that results in greater adsorption of AOc, i.e., the main interaction between AOc is given by the hydrogen bond between the carbonyl group and the Brønsted acid site, however, because it has a higher amount of catalytic sites the adsorption can also occur by the hydroxyl group and on the unsaturation (double bonds) causing steric and diffusion problems inside the pores. In addition, the presence of water formed as the product of the esterification reaction favors the less conversion to methyl oleate, due to the preferential adsorption of the water

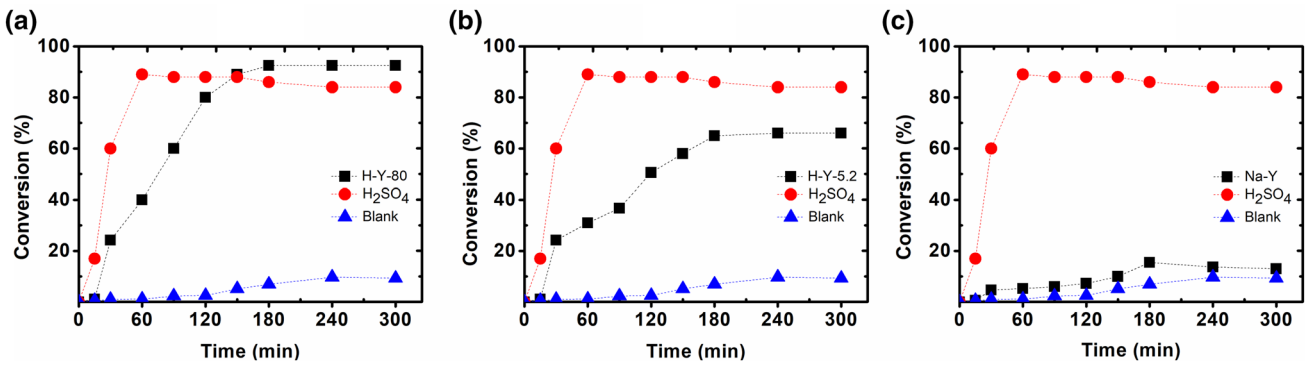

Fig. 5 Esterification of oleic acid on different catalysts. Conditions: MeOH/OAc molar ratio 3:1, 10 wt% catalyst, 100 °C

on the acid sites. Similar results are reported in the literature [23, 28] for Si/Al_3 molar ratio materials. It is also interesting to higligth that not all active sites can be accessed in FAU aluminosilicates [29], the accessibility of OAc to sites depends on spatial ordering and the environment in which are the active sites. Theoretical results (as discussed in detail in Sect. 3.3) predict the favorable accessibility for reactions involving OAc within FAU zeolites.

The conversion over Na-Y zeolite was lower when compared to H-Y-80, H-Y-5.2, that is only 15% of methyl oleate was obtained. It was observed that the catalytic activity is very similar to the non-catalytic reaction (Blank), showing that for the esterification of OAc on Na-Y (Si/Al = 2.6) is not active. This shows that only the accessibility of the reagent (AOc) to the interior of the pores and cavities is not the main factor to explain the catalytic process. The NH_3-TPD showed that this catalyst (Na-Y) did not present strong acid sites (Brønsted acid sites) only weak sites (Si–OH groups) in high concentration. The Brønsted acid sites in the conversion of FFA act on the carbonyl group promoting the adsorption and later the nucleophilic attack of the methanol molecule [15–17, 27], resulting in the formation of water and methyl ester. For Na-Y this reaction step does not occur due to the absence of strong acid sites.

Reaction rate for H_2SO_4 was more than H-Y-5.2 and Na-Y heterogeneous catalysts, showing a conversion of 89% OAc to methyl esters. But, H-Y-80 shows a higher conversion (92% vs. 89%). The better catalytic activity of H_2SO_4 has been reported previously in the esterification of acetic acid being attributed to the higher density of acid sites per gram of catalyst [4]. However, as the reaction progresses the catalytic activity of H_2SO_4 decreases gradually (approximately 5%). Possibly this effect can be related to the chemical equilibrium of the reaction, since the products formed in 60 min of reaction (H_2O and methyl ester) dislocate the equilibrium for the formation of reagents due to the hydrolysis. According to the literature [4, 46, 47], water production by the esterification impacts in the conversion of the product due to the decrease in the activity of the catalytic protons caused by the preferential solvation by the water presence in the reaction medium [46]. Autocatalysis process is not affected by the formation of water because the solvation of OAc in the liquid medium is low because it is considered a weak acid.

In order to understand the catalytic effects on the conversion of OAc on H-Y-80, H-Y-5.2 and Na-Y, it was analyzed the surface of the catalysts by ATR spectroscopy after 5 h of reaction, as shown in Fig. 6.

Low catalytic activity of Na-Y is evidenced by the presence of adsorbed water, characterized by the wide range between 3680-3095 cm^{-1} (νOH stretching) and 1643 cm^{-1} (axial deformation of δOH). It was observed that H-Y-80 and H-Y-5.2 did not showed bands related to water adsorbed

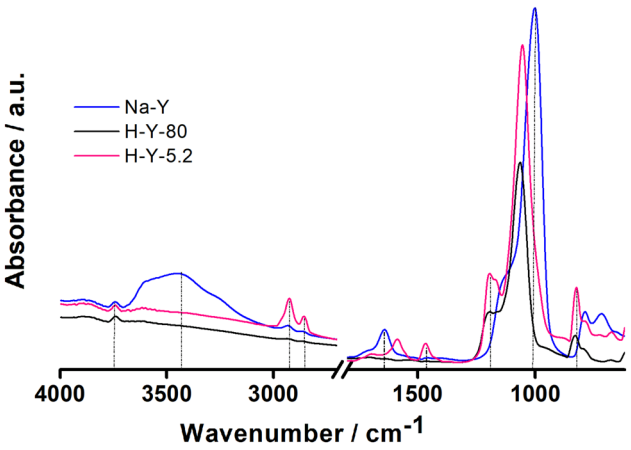

Fig. 6 IR spectra of FAU zeolite samples after 5 h of esterification with OAc and MeOH in the region of 4000–600 cm^{-1}

in the hydroxyl region, but the H-Y-5.2 zeolite presented on the surface adsorbed methyl groups (C–H), confirmed by the presence of bands at 2924–2856 cm^{-1} and two bands at 1587 and 1461 cm^{-1} (bending region). According to Vieira et al., [24] the presence of C–H groups (organic residues) adsorbed on the surface of aluminosilicates inhibits the catalytic activity. However, in H-Y-80 zeolite with higher Si/Al ratio, no water bands or adsorbed organic molecules were observed, only the presence of the Si–OH band at 3743 cm^{-1}, similar to the other catalysts (H-Y-5.2 and Na-Y). For all zeolites the 1300–600 cm^{-1} region was not discussed. According to Flaningen and Khatami regions below 1300 cm^{-1} indicate characteristics of subunits that form the FAU type zeolite structure [48].

6 Computational Results

Adsorption of acetic acid as a model molecule of FFA adsorbed on the Brønsted acid site showed that it is energetically favorable when it is compared to the MeOH adsorption, in a limiting step for the esterification reaction on the H-BEA zeolite [17]. In this context, the adsorption of OAc within the H-FAU cluster was investigated, as shown in Fig. 7.

High yield obtained experimentally for the esterification of OAc on H-Y-80 can be explained in greater details by the model of the electronic structure. It is observed that the FFA can be accommodated perfectly within the H-FAU zeolite, reaching the active site (Fig. 7). The molecular volume and the characteristic diameter for OAc were obtained according to the methodology presented by Herrmann and Iglesias [49]. The OAc volume derived from the theoretical results, and the molecular diameter is 18 nm^3 and 0.7 nm respectively (Fig. 7a). Size of the AOc has a significant

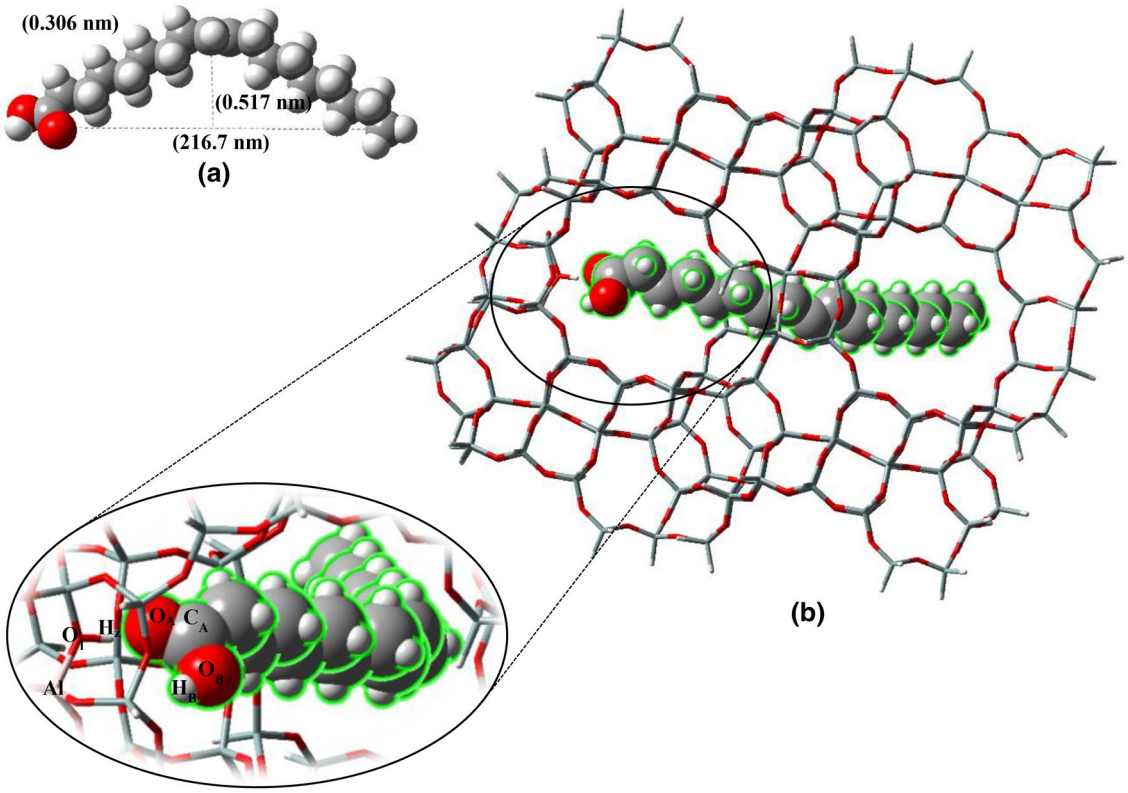

Fig. 7 Interactions between oleic acid and H-FAU zeolite cluster. **a** Estimation of the size of the oleic acid by DFT. **b** Oleic acid adsorbed complex in the H-FAU zeolite. Atom colorings are as follows: H in white, Si in gray, O in red and Al in pink

consequence within the cavity of zeolite H-FAU, because the confined environment surrounding the organic molecule distorts the increase of the van der Waals interactions between the catalyst framework and the organic molecule [50]. The OAc is stabilized by van der Walls interactions and is accommodated between the two large supercages that constitute the characteristic of the pores of the FAU structure (molecular dimensions of 1.2–1.3 nm that are bound by windows of approximately 0.74–0.8 nm of diameter composed of rings of 12 linked tetrahedral) [29, 30].

OAc adsorbed complex on the active site results in an adsorption energy of − 25.5 kJ mol^{-1}, similar values can be found for adsorption of acetic acid in H-ZSM-5 [51, 52] and in H-Beta [17]. No experimental value is found for the adsorption of oleic acid.

The main geometrical parameters and vibrational frequencies are presented in Table 1, before and after the adsorption of OAc.

According to Table 1, the bond distance O_1-H_Z increases from 9.7 to 10.1 nm as well as the angle Al-O_1-H_Z which increases 4°. The interaction between H_Z··· O_B shows a distance of 15.8 nm, and the νOH_Z vibrational frequency, displaces at a shorter wavelength from 3608 to 2833 cm^{-1}. This indicates a strong adsorption suggesting that the next step of the reaction would be the protonation of the fatty acid and consequently the formation of a chemisorbed intermediate.

For the OAc the C=O distance increases 0.2 nm in the adsorption, and the frequency νC=O displaces 94 cm^{-1} at the shorter wavelength, however the hydroxyl group (νOH_B) is identified at 3388 cm^{-1} being oriented to other

Table 1 Optimized geometrical parameters and harmonic vibrational frequencies for OAc and H-Y before and after physisorption on the Brønsted acid site calculated at ONIOM (M062X/6-31G (d):PM6) level

	Distances (nm)				Angles (º)	Frequency (cm^{-1})*		
	O_1–H_z	H_z···O_A	C_A=O_A	OH_b···O_z	Al-O_1-H_Z	νOH_Z	νC=O	νOH_B
OAc	–	–	12.0	–	–	–	1807	3562
H-FAU	9.7	–	–	–	112	3608	–	–
$Ads_{(OAc)}$	10.1	15.8	12.2	18.7	116	2833	1713	3388

ν stretching

*All frequencies are corrected by a factor of 0.947 [53]

O_z (oxygen atoms of the zeolite framework), indicating the formation of a weak H-bond between O and $H_B \cdots O_Z$, with a distance of 18.7 nm. The aliphatic chain presents an interesting effect as the intensity of the νCH_2 and νCH_3 frequencies in the region of 3007–2885 cm^{-1} decreases drastically indicating the stabilization of the large molecule due to several weak interactions inside the confined environments.

Summing up, the theoretical model predicts an indirect correlation between the pore diameter of the zeolite and the oleic acid molecule, that is, the voluminous confined space of the FAU zeolite perfectly accommodates the oleic acid molecule in the adsorption step. Despite being a bulky molecule, the fatty acid may have effective access to the inside the pores and the cavity of the zeolite in order to react on the active site within the channel.

7 Conclusion

In this work the catalytic activity of different FAU zeolites and H_2SO_4 in the esterification reaction of oleic acid was investigated through kinetic experiments and DFT calculations at the ONIOM (M062X/6-31G (d):PM6) level.

Results indicate that the catalytic activity of the different FAU zeolites is directly related to the distribution of the acid sites given by the Si/Al molar ratio within the pores and cavities. The effect of hydrophobicity on protonated zeolites with high Si/Al ratio (H-Y-80) showed to be beneficial for the esterification of OAc, resulting in high conversions of 92% methyl esters. On the other hand, it was observed by ATR spectroscopy that in the zeolites with low Si/Al ratio after 300 min of reaction the methyl groups (2924–2856 cm^{-1}) and water (3680–3095 and 1643 cm^{-1}) were adsorbed on the surface. This reflected the smaller conversions for H-Y-5.2 (66% conversion) and Na-Y (15% conversion). The reaction rate of H_2SO_4 was higher when compared to the acid zeolites, but the presence of water for more than 60 min resulted in the hydrolysis reaction and, consequently, the activity of the homogeneous acid catalyst decreased.

Detailed analysis of the theoretical results shows that the voluminous confined space of the FAU zeolite perfectly accommodates the OAc molecule in the adsorption step ($E_{ads} = -25.5$ kJ mol^{-1}) and the van der Waals interactions of the zeolite walls with the aliphatic chain help to accommodate the bulky molecule between the supercages with enough spaces. This should allow forming voluminous transition states that will give rise to the reaction.

Finally, experimental and theoretical results confirm that H-Y-80 zeolite applied in the esterification reaction can be an efficient catalyst in processes involving conversion of unsaturated fatty acids.

Acknowledgements This research was made possible by Consejo Nacional de Investigaciones Científicas y Técnicas (CONICET) and Secretaría General de Ciencia y Técnica of the Universidad Nacional del Nordeste (SGCyT-UNNE) of Argentine, and Coordenação de Aperfeiçoamento de Pessoal de Nível Superior (CAPES) of Brazil. The authors would also like to acknowledge Dr. Marcucci, S. M. P. and Ms. Duarte, V. A. at the Universidade Estadual de Maringá for his assistance in performing the CG-FID and NH_3-TPD measurements.

References

1. Wu L, Moteki T, Gokhale Amit A, Flaherty David W, Toste FD (2016) Production of fuels and chemicals from biomass: condensation reactions and beyond. Chem Biomol Eng 1(1):32–58. https://doi.org/10.1016/j.chempr.2016.05.002
2. Dusselier M, Davis ME (2018) Small-pore zeolites: synthesis and catalysis. Chem Rev 118(11):5265–5329. https://doi.org/10.1021/acs.chemrev.7b00738
3. Lilja J, Murzin DY, Salmi T, Aumo J, Mäki-Arvela P, Sundell M (2002) Esterification of different acids over heterogeneous and homogeneous catalysts and correlation with the Taft equation. J Mol Catal A 182–183:555–563. https://doi.org/10.1016/S1381-1169(01)00495-2
4. Liu Y, Lotero E, Goodwin JG (2006) A comparison of the esterification of acetic acid with methanol using heterogeneous versus homogeneous acid catalysis. J Catal 242(2):278–286. https://doi.org/10.1016/j.jcat.2006.05.026
5. Chouhan APS, Sarma AK (2011) Modern heterogeneous catalysts for biodiesel production: a comprehensive review. Renew Sustain Energy Rev 15(9):4378–4399. https://doi.org/10.1016/j.rser.2011.07.112
6. Lee AF, Bennett JA, Manayil JC, Wilson K (2014) Heterogeneous catalysis for sustainable biodiesel production via esterification and transesterification. Chem Soc Rev 43(22):7887–7916. https://doi.org/10.1039/C4CS00189C
7. Chouhan APS, Sarma AK (2011) Modern heterogeneous catalysts for biodiesel production: a comprehensive review. Renew Sustain Energy Rev 15(9):4378–4399. https://doi.org/10.1016/j.rser.2011.07.112
8. Semwal S, Arora AK, Badoni RP, Tuli DK (2011) Biodiesel production using heterogeneous catalysts. Bioresour Technol 102(3):2151–2161. https://doi.org/10.1016/j.biortech.2010.10.080
9. Gupta P, Paul S (2014) Solid acids: green alternatives for acid catalysis. Catal Today 236:153–170. https://doi.org/10.1016/j.cattod.2014.04.010
10. Sani YM, Daud WMAW, Abdul Aziz AR (2014) Activity of solid acid catalysts for biodiesel production: a critical review. Appl Catal A 470:140–161. https://doi.org/10.1016/j.apcata.2013.10.052
11. Ennaert T, Van Aelst J, Dijkmans J, De Clercq R, Schutyser W, Dusselier M, Verboekend D, Sels BF (2016) Potential and challenges of zeolite chemistry in the catalytic conversion of biomass. Chem Soc Rev 45(3):584–611. https://doi.org/10.1039/C5CS00859J
12. Resasco DE, Wang B, Crossley S (2016) Zeolite-catalysed C–C bond forming reactions for biomass conversion to fuels and chemicals. Catal Sci Technol 6(8):2543–2559. https://doi.org/10.1039/C5CY02271A
13. Corma A (2016) Heterogeneous catalysis: understanding for designing, and designing for applications. Angew Chem Int Ed 55(21):6112–6113. https://doi.org/10.1002/anie.201601231
14. Kirumakki SR, Nagaraju N, Narayanan S (2004) A comparative esterification of benzyl alcohol with acetic acid over zeolites

Hβ, HY and HZSM5. Appl Catal A 273(1–2):1–9. https://doi.org/10.1016/j.apcata.2004.03.016
15. Kirumakki SR, Nagaraju N, Chary KVR (2006) Esterification of alcohols with acetic acid over zeolites Hβ, HY and HZSM5. Appl Catal A 299:185–192. https://doi.org/10.1016/j.apcata.2005.10.033
16. Bedard J, Chiang H, Bhan A (2012) Kinetics and mechanism of acetic acid esterification with ethanol on zeolites. J Catal 290:210–219. https://doi.org/10.1016/j.jcat.2012.03.020
17. Gomes GJ, Zalazar MF, Lindino CA, Scremin FR, Bittencourt PRS, Costa MB, Peruchena NM (2017) Adsorption of acetic acid and methanol on H-Beta zeolite: an experimental and theoretical study. Microporous Mesoporous Mater 252:17–28. https://doi.org/10.1016/j.micromeso.2017.06.008
18. Aranda DAG, Gonçalves JdA, Peres JS, Ramos ALD, de Melo CAR, Antunes OAC, Furtado NC, Taft CA (2009) The use of acids, niobium oxide, and zeolite catalysts for esterification reactions. J Phys Org Chem 22(7):709–716. https://doi.org/10.1002/poc.1520
19. Hartmann M, Machoke AG, Schwieger W (2016) Catalytic test reactions for the evaluation of hierarchical zeolites. Chem Soc Rev 45(12):3313–3330. https://doi.org/10.1039/C5CS00935A
20. Carrero A, Vicente G, Rodríguez R, Linares M, del Peso GL (2011) Hierarchical zeolites as catalysts for biodiesel production from nannochloropsis microalga oil. Catal Today 167(1):148–153. https://doi.org/10.1016/j.cattod.2010.11.058
21. Fernandes DR, Rocha AS, Mai EF, Mota CJA, Teixeira da Silva V (2012) Levulinic acid esterification with ethanol to ethyl levulinate production over solid acid catalysts. Appl Catal A 425–426:199–204. https://doi.org/10.1016/j.apcata.2012.03.020
22. Chung K-H, Chang D-R, Park B-G (2008) Removal of free fatty acid in waste frying oil by esterification with methanol on zeolite catalysts. Bioresour Technol 99(16):7438–7443. https://doi.org/10.1016/j.biortech.2008.02.031
23. Chung K-H, Park B-G (2009) Esterification of oleic acid in soybean oil on zeolite catalysts with different acidity. J Ind Eng Chem 15(3):388–392. https://doi.org/10.1016/j.jiec.2008.11.012
24. Vieira SS, Magriotis ZM, Santos NAV, Saczk AA, Hori CE, Arroyo PA (2013) Biodiesel production by free fatty acid esterification using lanthanum (La^{3+}) and HZSM-5 based catalysts. Bioresour Technol 133:248–255. https://doi.org/10.1016/j.biortech.2013.01.107
25. Vieira SS, Magriotis ZM, Ribeiro MF, Graça I, Fernandes A, Lopes JMFM, Coelho SM, Santos NAV, Saczk AA (2015) Use of HZSM-5 modified with citric acid as acid heterogeneous catalyst for biodiesel production via esterification of oleic acid. Microporous Mesoporous Mater 201:160–168. https://doi.org/10.1016/j.micromeso.2014.09.015
26. Vieira SS, Magriotis ZM, Graça I, Fernandes A, Ribeiro MF, Lopes JMFM, Coelho SM, Santos NAV, Saczk AA (2017) Production of biodiesel using HZSM-5 zeolites modified with citric acid and SO_4^{2-}/La_2O_3. Catal Today 279(2):267–273. https://doi.org/10.1016/j.cattod.2016.04.014
27. Prinsen P, Luque R, González-Arellano C (2018) Zeolite catalyzed palmitic acid esterification. Microporous Mesoporous Mater 262:133–139. https://doi.org/10.1016/j.micromeso.2017.11.029
28. Doyle AM, Albayati TM, Abbas AS, Alismaeel ZT (2016) Biodiesel production by esterification of oleic acid over zeolite Y prepared from kaolin. Renew Energy 97:19–23. https://doi.org/10.1016/j.renene.2016.05.067
29. Busca G (2017) Acidity and basicity of zeolites: a fundamental approach. Microporous Mesoporous Mater 254:3–16. https://doi.org/10.1016/j.micromeso.2017.04.007
30. Kaduk JA, Faber J (1995) Crystal structure of zeolite Y as a function of ion exchange. Rigaku J 12(2):14–34
31. Corma A, Garcia H, Iborra S, Primo J (1989) Modified faujasite zeolites as catalysts in organic reactions: esterification of carboxylic acids in the presence of HY zeolites. J Catal 120(1):78–87. https://doi.org/10.1016/0021-9517(89)90252-2
32. Bouguerra Neji S, Trabelsi M, Frikha M (2009) Esterification of fatty acids with short-chain alcohols over Commercial acid clays in a semi-continuous reactor. Energies 2(4):1107
33. Doyle AM, Alismaeel ZT, Albayati TM, Abbas AS (2017) High purity FAU-type zeolite catalysts from shale rock for biodiesel production. Fuel 199:394–402. https://doi.org/10.1016/j.fuel.2017.02.098
34. Verstraelen T, Van Speybroeck V, Waroquier M (2008) ZEOBUILDER: a GUI toolkit for the construction of complex molecular structures on the nanoscale with building blocks. J Chem Inf Model 48(7):1530–1541. https://doi.org/10.1021/ci8000748
35. Maseras F, Morokuma K (1995) IMOMM: a new integrated ab initio + molecular mechanics geometry optimization scheme of equilibrium structures and transition states. J Comput Chem 16(9):1170–1179. https://doi.org/10.1002/jcc.540160911
36. Chung LW, Sameera WMC, Ramozzi R, Page AJ, Hatanaka M, Petrova GP, Harris TV, Li X, Ke Z, Liu F, Li H-B, Ding L, Morokuma K (2015) The ONIOM method and its applications. Chem Rev 115(12):5678–5796. https://doi.org/10.1021/cr5004419
37. Zalazar MF, Paredes EN, Romero Ojeda GD, Cabral ND, Peruchena N (2018) Study of confinement and catalysis effects of the reaction of methylation of benzene by methanol in H-beta and H-ZSM-5 zeolites by topological analysis of electron density. J Phys Chem C 122(6):3350–3362. https://doi.org/10.1021/acs.jpcc.7b10297
38. Frisch MJ, Trucks GW, Schlegel HB, Scuseria GE, Robb MA, Cheeseman JR, Montgomery JA, Vreven T, Kudin KN, Burant JC, Millam JM, Iyengar SS, Tomasi J, Barone V, Mennucci B, Cossi M, Scalmani G, Rega N, Petersson GA, Nakatsuji H, Hada M, Ehara M, Toyota K, Fukuda R, Hasegawa J, Ishida M, Nakajima T, Honda Y, Kitao O, Nakai H, Klene M, Li X, Knox JE, Hratchian HP, Cross JB, Adamo C, Jaramillo J, Gomperts R, Stratmann RE, Yazyev O, Austin AJ, Cammi R, Pomelli C, Ochterski JW, Ayala PY, Morokuma K, Voth GA, Salvador P, Dannenberg JJ, Zakrzewski G, Dapprich S, Daniels AD, Strain MC, Farkas O, Malick DK, Rabuck AD, Raghavachari K, Foresman JB, Ortiz JV, Cui Q, Baboul AG, Clifford S, Cioslowski J, Stefanov BB, Liu G, Liashenko A, Piskorz P, Komaromi I, Martin RL, Fox DJ, Keith T, Al-Laham MA, Peng CY, Nanayakkara A, Challacombe M, Gill PMW, Johnson B, Chen W, Wong MW, Gonzalez C, Pople JA (2009) Gaussian 09, Revision A.01 edn. Gaussian, Inc, Wallingford
39. Bordiga S, Lamberti C, Bonino F, Travert A, Thibault-Starzyk F (2015) Probing zeolites by vibrational spectroscopies. Chem Soc Rev 44(20):7262–7341. https://doi.org/10.1039/C5CS00396B
40. Salman N, Rüscher CH, Buhl JC, Lutz W, Toufar H, Stöcker M (2006) Effect of temperature and time in the hydrothermal treatment of HY zeolite. Microporous Mesoporous Mater 90(1):339–346. https://doi.org/10.1016/j.micromeso.2005.09.032
41. Zhao J, Yin Y, Li Y, Chen W, Liu B (2016) Synthesis and characterization of mesoporous zeolite Y by using block copolymers as templates. Chem Eng J 284:405–411. https://doi.org/10.1016/j.cej.2015.08.143
42. Murphy B, Davis ME, Xu B (2015) The effect of adsorbed molecule gas-phase deprotonation enthalpy on ion exchange in sodium exchanged zeolites: an in situ FTIR investigation. Top Catal 58(7):393–404. https://doi.org/10.1007/s11244-015-0383-z
43. Guisnet M, Guidotti M (2006) Catalysts for fine chemical synthesis: microporous and mesoporous solid catalysts. In: Roberts

EGDSM (ed) Microporous and mesoporous solid catalysts, vol 4. Wiley, New York, pp 39–67
44. Arca HA, Mota CJA (2018) Rearrangement of cyclopropylcarbinyl chloride over protonic zeolites: formation of carbocations and behavior as solid solvents. Top Catal 61(7):616–622. https://doi.org/10.1007/s11244-018-0911-8
45. Mistry SR, Joshi RS, Sahoo SK, Maheria KC (2011) Synthesis of dihydropyrimidinones using large pore zeolites. Catal Lett 141(10):1541–1547. https://doi.org/10.1007/s10562-011-0639-6
46. Liu Y, Lotero E, Goodwin JG (2006) Effect of water on sulfuric acid catalyzed esterification. J Mol Catal A 245(1):132–140. https://doi.org/10.1016/j.molcata.2005.09.049
47. Marchetti JM, Errazu AF (2008) Comparison of different heterogeneous catalysts and different alcohols for the esterification reaction of oleic acid. Fuel 87(15):3477–3480. https://doi.org/10.1016/j.fuel.2008.05.011
48. Flanigen EM, Khatami H, Szymanski HA (1974) Infrared structural studies of zeolite frameworks. Advances in Chemistry, vol 101. Molecular sieve zeolites-I. American Chemical Society, Washington, pp 201–229
49. Herrmann S, Iglesia E (2017) Elementary steps in acetone condensation reactions catalyzed by aluminosilicates with diverse void structures. J Catal 346:134–153. https://doi.org/10.1016/j.jcat.2016.12.011
50. Sarazen ML, Iglesia E (2018) Effects of charge, size, and shape of transition states, bound intermediates, and confining voids in reactions of alkenes on solid acids. ChemCatChem 10(18):4028–4037. https://doi.org/10.1002/cctc.201800401
51. Yan H, Feng X, Liu Y, Yang C, Shan H (2017) Catalytic cracking of acetic acid and its ketene intermediate over HZSM-5 catalyst: a density functional theory study. Mol Catal 437:11–17. https://doi.org/10.1016/j.mcat.2017.04.038
52. Gomes GJ, Zalazar MF, Arroyo PA, Scremin FR, Costa MB, Bittencourt PRS, Lindino CA, Peruchena NM (2019) Molecular-level understanding of the rate-determining step in esterification reactions catalyzed by H-ZSM-5 Zeolite. An experimental and theoretical study. ChemSelect 4(11):3031–3041. https://doi.org/10.1002/slct.201900689
53. Kesharwani MK, Brauer B, Martin JML (2015) Frequency and zero-point vibrational energy scale factors for double-hybrid density functionals (and other selected methods): can anharmonic force fields be avoided? J Phys Chem A 119(9):1701–1714. https://doi.org/10.1021/jp508422u